ORIGINAL PAPER

Effects of continuous cooling rate on morphology of granular bainite in pipeline steels

Shu-jun Jia[1] · Ba Li[1] · Qing-you Liu[1] · Yi Ren[2] · Shuai Zhang[2] · Hong Gao[2]

Abstract

The morphology and characteristics of granular bainite (GB) in pipeline steels at different continuous cooling rates were investigated by scanning electron microscopy, transmission electron microscopy and electron back-scattered diffraction (EBSD). The results show that the morphology of ferrite matrix in GB turned from the lath sheaf structure into the nearly equiaxed large grain with the cooling rate decreasing from high (60 °C/s) to low (5–10 °C/s). At the medium cooling rate (20–40 °C/s), GB consisted of the irregular ferrite matrix, the granular martensite/austenite (M/A) constituents and abundant substructures inside. The formation of the irregular ferrite and substructure was attributed to the high-temperature recovery which occurred at relatively high-temperature stage before phase transformation. The granular morphology of M/A constituents was formed from the carbon-rich triple junctions which were produced by the multidirectional substructure interfaces converged with each other. Particularly, some martensite in M/A constituents was misoriented from the adjacent ferrite by very small misorientation angle, which could be characterized by the mean band contrast function of EBSD qualitatively or semiquantitatively.

Keywords Granular bainite · Continuous cooling · M/A constituent · Cooling rate · Irregular substructure

1 Introduction

The granular bainite composed of the equiaxed bainitic ferrite matrix and island constituents was firstly found in low- and medium-carbon alloyed steels [1]. The island constituent, named martensite/austenite (M/A) constituent, was composed of martensite and retained austenite originally transforming from carbon-rich austenite partially to martensite during subsequent cooling process. The granular bainite (GB) microstructure can generally be produced under the process of continuous cooling [2]. In the industrial production, steel is mainly produced under the condition of continuous cooling. Therefore, the GB microstructure gives rise to the great interest in industry. It is reported that the

strength and toughness of low-carbon GB steel were higher than those of ferrite–pearlite steel resulted from the combination of grain refinement and dislocation strengthening (substructure strengthening) [3, 4].

To date, the understanding of GB microstructure has not reached a consensus, and its transformation mechanism is also indistinct. Particularly in the pipeline steels, products of the non-equilibrium phase transformation usually contain little cementite due to the extremely low carbon content [1, 5, 6]. In this case, the final microstructure tends to form ferrite rather than bainite and normally consists of various morphologies of ferrite, such as polygonal ferrite (PF), quasi-polygonal ferrite (QF), granular bainitic ferrite (GB), acicular ferrite (AF) and bainitic ferrite (BF) [7–10]. As a result, the definition of GB microstructure is confusing in pipeline steel, which is sometimes considered as BF or AF microstructure [3, 10–13]. Actually, due to relatively similar range of phase transformation temperature, the deformed austenite can be transformed to multifarious ferrite under the continuous cooling process. It means that the phase transformation regions of different kinds of ferrite are overlapped during continuous cooling, further increasing the difficulty in identifying microstructure [6, 14, 15].

✉ Ba Li
  balicugb@sina.com

1 Department of Structural Steels, Central Iron and Steel Research Institute, Beijing 100081, China

2 State Key Laboratory of Metal Material for Marine Equipment and Application of Iron and Steel Research Institutes of Ansteel Group Corporation, Anshan 114009, Liaoning, China

Thompso et al. [16] reported a GB microstructure consisting of granular morphology M/A constituents or as-retained austenite and a featureless matrix with reserved prior austenite grain boundary, which could be formed during continuous cooling process. Caballero et al. [17] revealed that the transformation mechanism of GB was similar to that of the lath-like bainite, while the lath structure in GB is coarse or incomplete. However, Zajac et al. [18] found that the ferrite matrix of GB had irregular grain boundary and often showed the etching evidence that the dislocation substructures constrain the retained austenite into equiaxed shape.

Since the above reasons illustrate the complexity of the GB microstructure in pipeline steel, it is necessary to systematically investigate the morphologic characterization and the corresponding influence factors.

2 Experimental material and procedures

The commercial high-grade pipeline steel was used in this work. Its chemical composition was C 0.04, Si 0.28, Mn 1.54, P 0.011, S 0.002, Nb 0.062, Ti 0.014, Mo 0.14, Ni 0.29, Cr 0.25 and Fe balance (in wt.%). The pipeline steel cylindrical tubes with a diameter of 8 mm and a length of 20 mm were adopted to ensure enough deformation. The process of thermal simulation test is illustrated in Fig. 1. The cylindrical tubes were firstly austenitized for 300 s at 1180 °C and then performed two-stage deformations by 25% at 980 °C and 60% at 820 °C in turn. Finally, the deformed specimens were cooled to room temperature at the linear cooling rates of 1, 2, 5, 10, 20, 40 and 60 °C/s, respectively. A combination of scanning electron microscopy (SEM, S-4300) and transmission electron microscopy (TEM, H-800) was adopted to investigate the morphology of GB in detail. The characteristic of interior substructure of GB
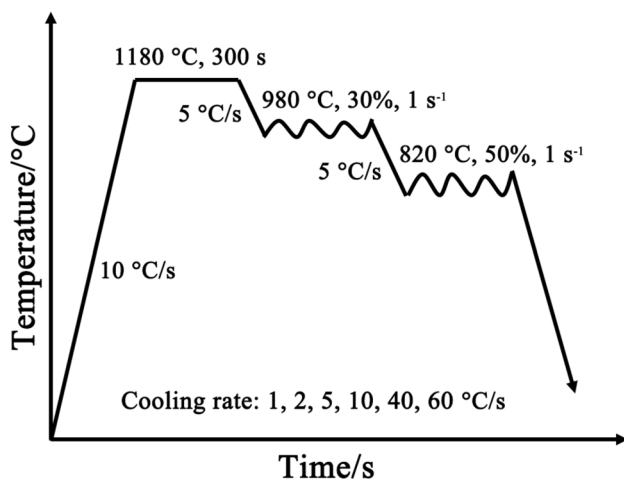
was carried out by TEM. The crystallographic information was provided by electron back-scattered diffraction (EBSD, Nordlys F+). The longitudinal section of samples for optical microscopy (OM, MEF-4M) and SEM was ground and polished and then etched in a 4 vol.% Nital solution. The thin-foil samples for TEM were electropolished by twin-jet electropolisher in an electrolyte consisting of 6 vol.% perchloric acid and 94 vol.% alcohol at − 30 °C. The EBSD samples were electropolished using the electrolyte with 10 vol.% perchloric acid and 90 vol.% acetic acid.

3 Results and discussion

3.1 GB morphology under different cooling rates

In general, the BF in pipeline steels commonly contains the sheaf structures with parallel laths surrounded by parent austenite grain boundary (PAGB) [17]. In contrast to the BF, AF microstructure is described as a non-equiaxed ferrite matrix with relatively high dislocation density and distributed in a random manner, which always contains interwoven ferrite plates with high aspect ratio [19]. As shown in Fig. 2a, BF cannot be found even at the fastest cooling rate. The final microstructure was mixed with AF and GB. This phenomenon is in accordance with the former studies that BF microstructure is restricted under large deformation in the austenite non-recrystallization region [12, 20]. The AF and GB were also mixed together at cooling rate of 40 °C/s, as shown in Fig. 2b. GB and AF could be simultaneously observed because both of them phase-transformed in similar temperature range during continuous cooling process [21]. Particularly, due to the widening of the AF plates with decreasing cooling rate, the morphology became indistinguishable in some region. At the cooling rate of 20 °C/s, GB consisted of the irregular ferrite and granular M/A islands, which was one of the typical morphologies of GB. As the cooling rate decreased from 10 to 2 °C/s, as shown in Fig. 2d–f, the ferrite matrix was changed to the equiaxed morphology and the grain boundaries became clear and straight. At the cooling rate of 5 °C/s (Fig. 2e), a large number of QF grains were formed and the M/A constituents turned into the dot-like particles which were distributed on both grain interior and grain boundary. At the lowest cooling rate of 2 °C/s, the microstructure was dominated by PF and QF, as shown in Fig. 2f. According to the OM images, the dynamic continuous cooling transformation (CCT) diagram was constructed and is displayed in Fig. 3a, which shows the microstructural evolution with variation of cooling rate. In addition, the microhardness of samples at different cooling rates is displayed in Fig. 3b, which decreased with the decreasing cooling rate. Observed from the microstructure
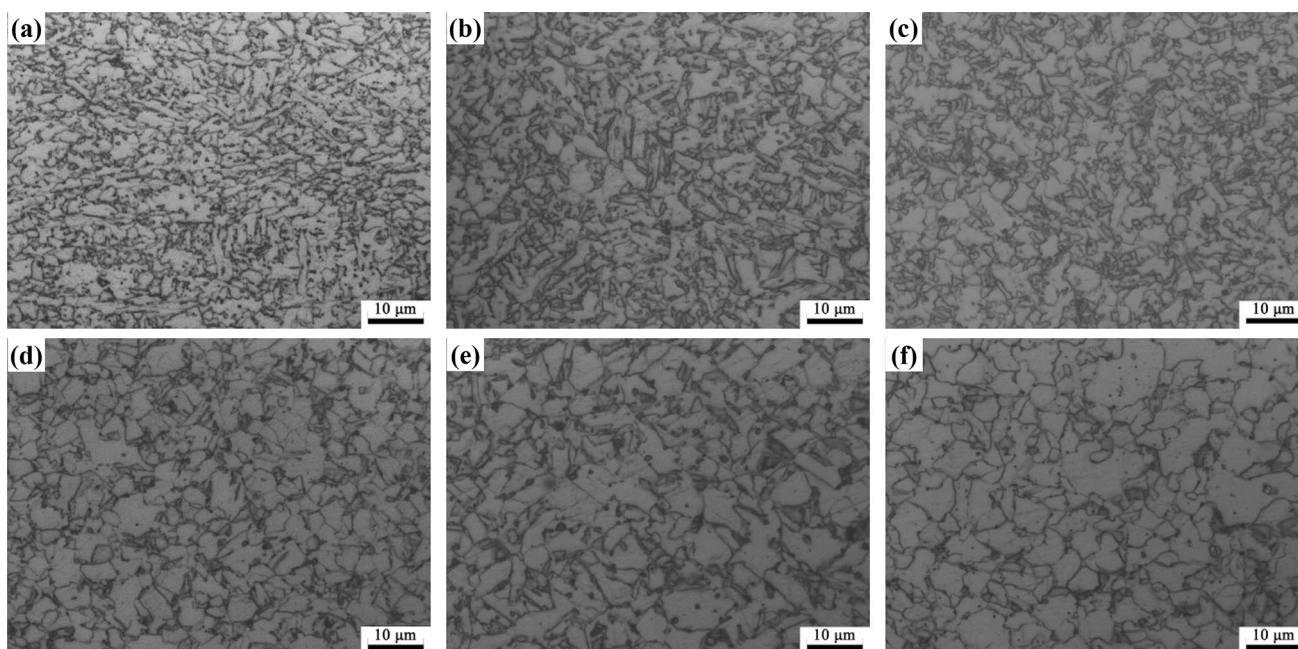

Fig. 1 Schematic diagram of thermal simulation process

Fig. 2 Optical micrographs of samples at different cooling rates. **a** 60 °C/s; **b** 40 °C/s; **c** 20 °C/s; **d** 10 °C/s; **e** 5 °C/s; **f** 2 °C/s
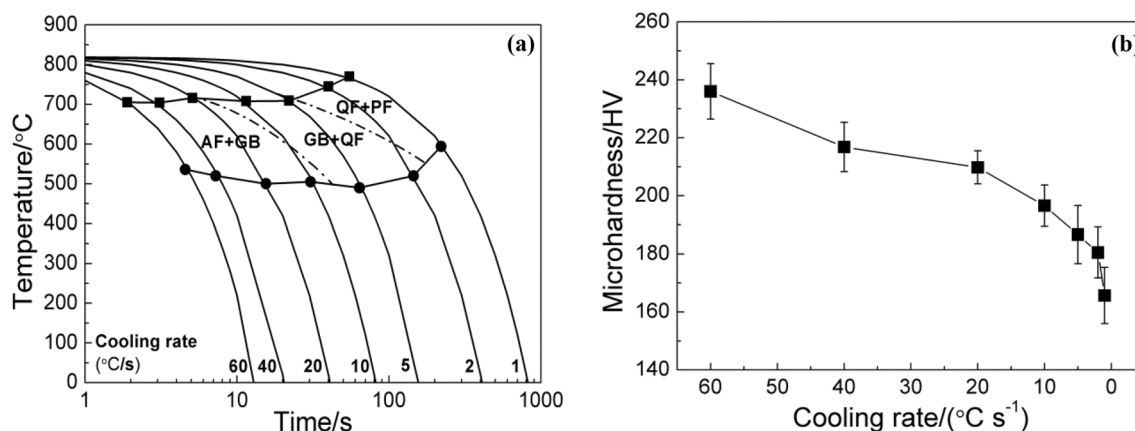

Fig. 3 Dynamic continuous cooling transformation diagrams (**a**) and microhardness of samples at different cooling rates (**b**)

above, the mixed microstructure of AF and GB cannot be distinguished clearly in OM.

For characterizing the elaborate structure of the mixture microstructure, Fig. 4 shows the typical SEM morphology of GB at different cooling rates, which presents the characteristics of the ferrite matrix and M/A constituents. At the high cooling rate of 60 °C/s (Fig. 4a), a large equiaxed GB grain was made up of three coarsened ferrite blocks. The nearly parallel M/A constituents in one of the blocks implied the existence of lath structures inside. The granular M/A constituents appeared at grain, block and lath boundaries; especially, a long-strip M/A constituent distributed along the grain boundaries. Then, the granular and long-strip M/A

constituent as well as the normal grain boundaries together made up the complete PAGB. However, in Fig. 4b, only part of PAGB remained and the short rod-shaped M/A constituents with approximately parallel arrangement in GB showed the sheaf morphology. The etching evidence of dislocation substructures helped to draw the outline of the sheaf structure. Therefore, at the high cooling rate, GB consisted of the rough ferrite lath or sheaf structure and the M/A constituents with granular or short rod shape; meanwhile, the PAGB could be completely or partly remained. At the medium cooling rate corresponding to 40 and 20 °C/s in Fig. 4c, d, the GB grains were refined dramatically and turned into the featureless morphology with the granular
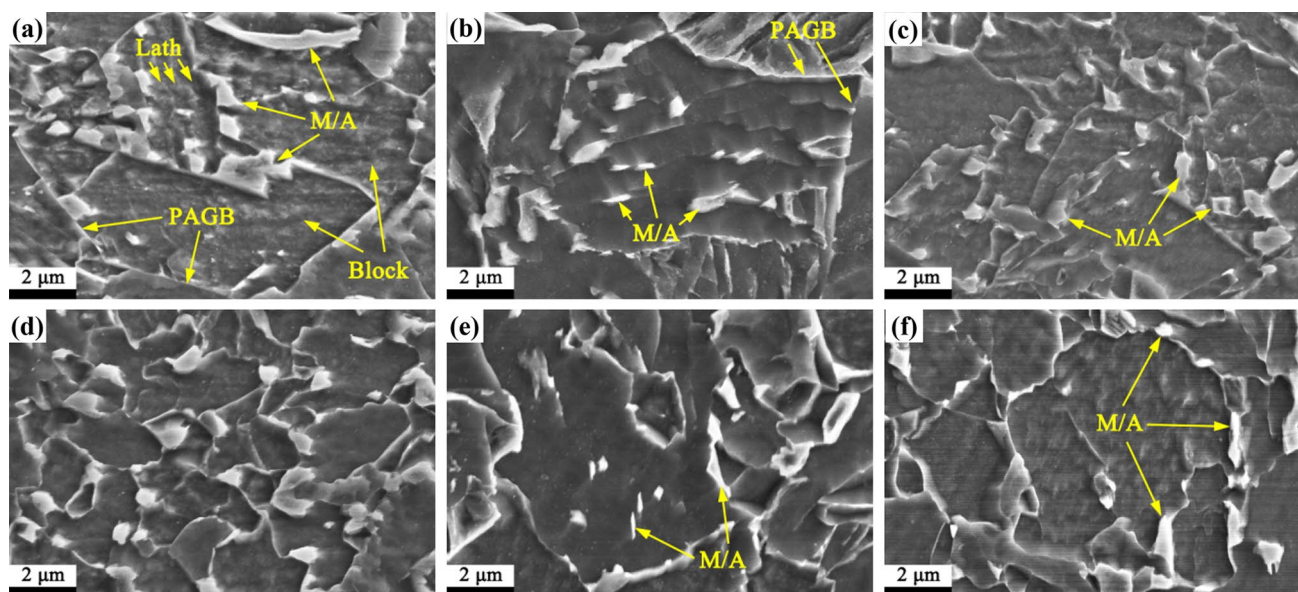
Fig. 4 Scanning electron micrographs of GB microstructures at different cooling rates. **a**, **b** 60 °C/s; **c** 40 °C/s; **d** 20 °C/s; **e** 10 °C/s; **f** 5 °C/s

M/A constituents distributing on the grain boundaries or the triple junctions. The distribution of the irregular ferrite and granular M/A constituents was more uniform at 20 °C/s compared with that at 40 °C/s. At the relatively low cooling rate of 10 and 5 °C/s, the ferrite matrix of GB became quite large and equiaxial, whereas the fraction of the M/A constituents decreased and their size reduced, as shown in Fig. 4e, f. Caballero et al. [17] remarked that the GB microstructure observed as granular coarse ferrite plate with M/A islands via OM and SEM did not really exist; the GB actually consisted of bainite ferrite sheaves and very fine austenite between the subunits. In the present work displayed in Fig. 4, three kinds of typical morphologies of GB can be distinguished at different cooing rates using high-resolution SEM.

For further investigating the elaborate structure of GB microstructure, the TEM graphs were displayed and analyzed. The typical TEM morphology of GB at different cooling rates is shown in Fig. 5. At 60 °C/s, the sheaf structures with fine laths were detected and the M/A constituents formed on the top of the laths, as shown in Fig. 5a. At the same time, the rough ferrite laths are also observed in Fig. 5b, which consisted of the strip-type and film-type M/A constituents. The growth of ferrite laths terminated at the PAGB or the adjacent lath boundaries, which boosted carbon in enriching at the grain or lath boundaries, resulting in the formation of the two types of M/A constituents.

The ferrite laths contained high-density dislocations, as indicated in Fig. 5c. These observations contribute to elucidating shearing mechanism during GB transformation under the high cooling rate [22].

At the medium cooling rates varying from 40 to 20 °C/s, the lath of sheaf structures in matrix was replaced by the nearly equiaxed substructures with the granular M/A constituents inside, as shown in Fig. 5d–f, which is in accordance with the results of SEM. The high-density dislocations in ferrite matrix were partly tangled together, which formed the dislocation cells and subgrains. The abundant substructures indicate that the significant recovery process was underway during continuous cooling with the medium rate. These well-developed substructures could restrict the following bainite transformation, which destroyed the lath sheaf structures of bainitic ferrite.

At the low cooling rate of 10 and 5 °C/s (Fig. 5g–i), the dislocation tangle and annihilation processes would sustain for a long time, resulting in the dislocation density decreasing and the substructure coarsening. At these cooling rates, the content of carbon atoms which are on both the grain and subgrain boundaries declined obviously due to carbon diffusion. Then, many QF microstructures were transformed, which had relatively low dislocation density and large grain size. Meanwhile, the grain size and fraction of the M/A constituents decreased significantly. Fang et al. [23] suggested that the so-called "granular bainite" includes two kinds of microstructures: one was ferrite matrix with PAGB which possessed lath sheaves and semi-continuous strip-shaped islands distributed in lath and grain boundaries; and the other called granular structure, in which the ferrite matrix was composed of irregular massive pro-eutectoid ferrite and featureless islands with random distribution. Therefore, referring to their classification of GB, in present work, the GB microstructure produced under the high cooling rate
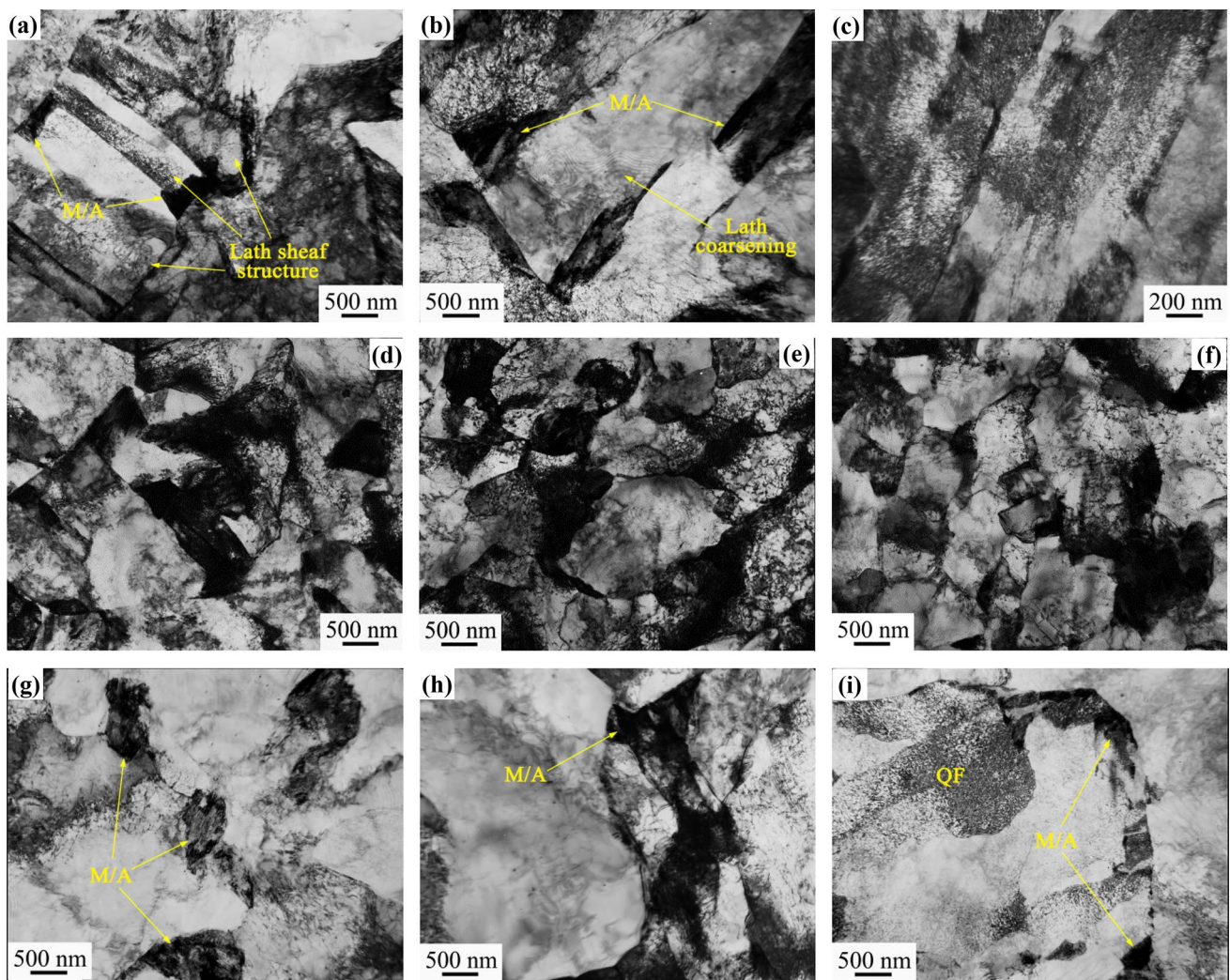
Fig. 5 Transmission electron micrographs of GB microstructures at different cooling rates. **a–c** 60 °C/s; **d** 40 °C/s; **e, f** 20 °C/s; **g, h** 10 °C/s; **i** 5 °C/s

was corresponding to the characteristics of granular bainite. The GB microstructure formed at the low cooling rate was similar to the granular structure. Fang et al. [23] pointed out that the strength of the GB was superior to that of granular structure, which is in accordance with the microhardness results shown in Fig. 3b, because the granular structure had a larger grain size with relatively low dislocation density comparing with GB.

Based on the results of SEM and TEM, it can be concluded that the GB morphology in pipeline steel changed with the cooling rate during continuous cooling. At a high cooling rate (60 °C/s), GB consisted of the complete or partial PAGB and obvious lath sheaf structure, and the strip-type and film-type M/A constituents were distributed on both the PAGBs and lath boundaries.

At a low cooling rate (10 or 5 °C/s), both the ferrite matrix and the inner substructures turned into large size,

nearly equiaxed shape and low dislocation density, while the lath sheaf structures disappeared. This can be called granular structure.

However, for a medium cooling rate (40 or 20 °C/s), the GB microstructure is complicated, which consisted of the irregular refined ferrite matrix and granular M/A constituents distributed on both grain and subgrain boundaries. Meanwhile, the sheaf structure and PAGB were hardly observed. These features were easily misunderstood as the AF microstructure, which also contained the non-equiaxed grains [5, 19]. Currently, few studies go ahead for a unified understanding of the formation process with respect to the GB morphology at the medium cooling rate. Therefore, this process will be discussed in the next section.

3.2 Formation of GB with irregular-shaped ferrite + granular M/A constituent

In order to investigate the formation process of GB transformed at the medium cooling rate, some typical microstructures were selected from the GB microstructure at 20 °C/s and are displayed in Fig. 6, which could form under the different states of the continuous cooling process. These microstructural characteristics could provide information of both the substructure variation and phase transformation during continuous cooling.

The deformation is inhomogeneous under a large degree of strain in the non-recrystallization region; as a result, the dislocation tangled and piled up together (Fig. 6a), forming the dislocation cell structures (Fig. 6b). At the high-temperature stage of the continuous cooling process, the dislocation cell walls are flattened by the cross-slip of the screw dislocations and the climb of the edge dislocations (Fig. 6c). It concludes that the polygonization process is

well developed, which is the main mechanism of the high-temperature recovery [24]. This process took place at the relatively high temperature before phase transformation, which boosted the formation of the featureless substructure (Fig. 6d). It is noteworthy that the substructures could also impinge with each other during the continuous cooling or transformation processes, which impels promoting the structure more disordered [19].

The presence of the irregular substructures will limit or destroy the development of the lath sheaf structures in the following bainite transformation. Meanwhile, the abundant substructures can also divide the parent austenite grain, resulting in the refinement of the whole microstructure, as shown in Figs. 4d and 5e, f.

When undercooling to the austenite decomposition temperature, the ferrite grain nucleuses commonly have a certain coherent relationship with parent austenite [22]. The coherent interface has so low energy that can be preferentially developed to make the ferrite grains in strip-typed form, as
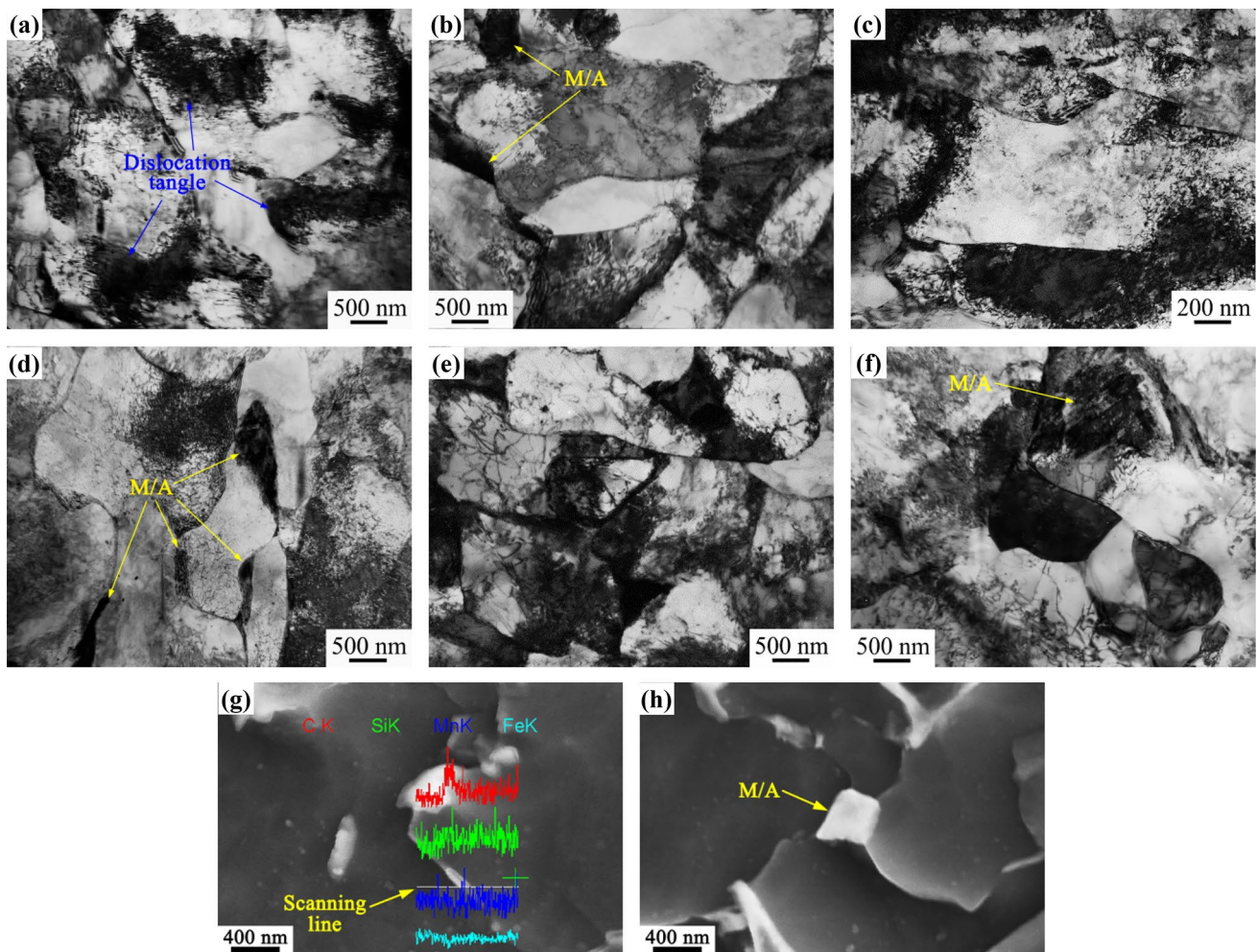

Fig. 6 Microstructure analysis for GB microstructure at 20 °C/s. a–d Typical TEM morphology of recovered structure during continuous cooling; e, f typical morphology of GB; g line scanning of interface; h granular M/A constituent formed on interface intersection

displayed in Fig. 6e. With the grain growth, the coherent relationship of interfaces loses gradually due to the restriction of the various substructures around. On the other hand, austenite under heavy deformation within non-recrystallized region could be transformed to ferrite through a high transforming rate, resulting from two factors: the high internal energy of the deformed austenite and the large number of nucleation sites provided by the deformed defects [6–8]. Due to the two factors, the aspect ratio development of the strip-typed ferrite grains was dynamically restricted, resulting in the microstructure further equiaxed and refined. As a result, both the irregular (Fig. 6d) and relatively equiaxed (Fig. 6f) ferrites can be produced resulting from the constraint of the abundant irregular substructures and rapid phase transformation. Moreover, defects caused by deformation can be inherited in GB at the high transformation rate [7, 11]. Thus, the GB matrix finally contains relatively high dislocation density, as shown in Figs. 5e, f and 6d, e.

In Fig. 6d, the strip-typed M/A constituents distributed along the substructure boundaries, which indicated that carbon aggregated unevenly at the preformed substructure interfaces. A line scan of the interface test was carried out via energy dispersive X-ray spectroscopy in SEM in Fig. 6g, which presented a distinct peak of the carbon element close to the interface front, i.e., the carbon accumulated at the interfaces. The development of the multidirectional substructure interfaces produced many triple junctions. Then, carbon was strongly accumulated at these triple junctions, which enhanced the austenite stability in these carbon-rich regions. Meanwhile, these regions tended to be equiaxed morphology at the multidirectional stress. Finally, the granular M/A constituents were formed at the triple junctions marked by the arrow in Fig. 6h. Cheprasov et al. [25] also reported that the density of defects accumulated around the globular carbides was an order of magnitude higher than the mean values, which had confirmed that the presence of elevated defect density in austenite dynamically enriched with carbon promoting the formation of globular carbide phase.

Furthermore, accompanied by the decrease in the whole grain and substructure size, the amount of the grain boundary nodes goes upward with the increasing carbon-enriched regions. As a result, the size of carbon-rich regions reduced. In other words, the grain size of the M/A constitutes is refined. It is accepted that the existence of a very hard phase (such as martensite) in microstructure deteriorates the toughness [26]. Some researchers stated that GB was a harmful microstructure which should be avoided due to the reduction in toughness of steels [4, 27]. However, Caballero et al. [17] reported that the critical size of M/A constitutes in GB to not crack easily should be controlled below ~ 10 μm. Fang et al. [23] also pointed out that the size of the M/A constitutes diminished with the decrease in the prior austenite grain size, which could improve the strength and toughness.

Therefore, it can be expected that the GB microstructures produced at the medium cooling rate possess excellent strength and toughness.

Considering the symbolic function of M/A constituents for GB, its morphology at the medium cooling rate is further characterized by SEM, TEM and EBSD in the next section.

3.3 Morphology of M/A constituents observed at medium cooling rate

Figure 7 displays the various distribution sites of the M/A constituents at the medium cooling rate. In the enlarged SEM image, the granular and strip-shaped M/A constituents presented the white light colors, which distributed on the triple junction of grains (see Fig. 7a), subgrain boundaries (see Fig. 7b) and matrix interior (see Fig. 7c). The M/A constituents caved in the ferrite matrix were smaller than those distributed on the interface nodes, indicating that more carbon element enriched at the various interface nodes.

For TEM, the M/A constituents commonly consisted of black and gray areas. As shown in Fig. 7d–g, there were a large amount of dislocations at the vicinity of the M/A constituents. This is mainly attributed to the martensite phase transformation when the M/A constituents were generated [28]. Some small austenite regions were carved in the ferrite matrix, which increased the interface area between the carved austenite and surrounding ferrite. Then, more carbon elements enriched in these small austenite regions, resulting in the formation of M/A constituents in the grain interior, as shown in Fig. 7f. Li et al. [29] also reported that the formation of the interior M/A constitutes was attributed to the generation of the carbon-rich and carbon-depleted zones in the deformed austenite.

Although there are some strip-typed M/A constituents, the granular-typed morphology is still dominated in GB microstructure. Particularly, Fig. 7h presents a kind of typical M/A constituents with micro-twinning which resulted from the retained austenite with high carbon content transforming to the twinned martensite.

Figure 8a shows the orientation map of the sample at 40 °C/s, in which GB microstructure predominated and contained the irregular substructures. The orientation maps defined a much larger grain size than that visualized with the OM micrograph. This phenomenon has already been accepted by other researches [9, 12, 30].

Chen et al. [31] studied the phase quantification between GB and ferrite using the kernel average misorientation function of EBSD. Lee et al. [32] distinguished the microstructure between GB and QF through the grain orientation spread function of EBSD. In addition to the two methods, the grain average misorientation and grain aspect ratio function of EBSD are used in combination to classify the various austenite decomposition products in microalloyed steels such
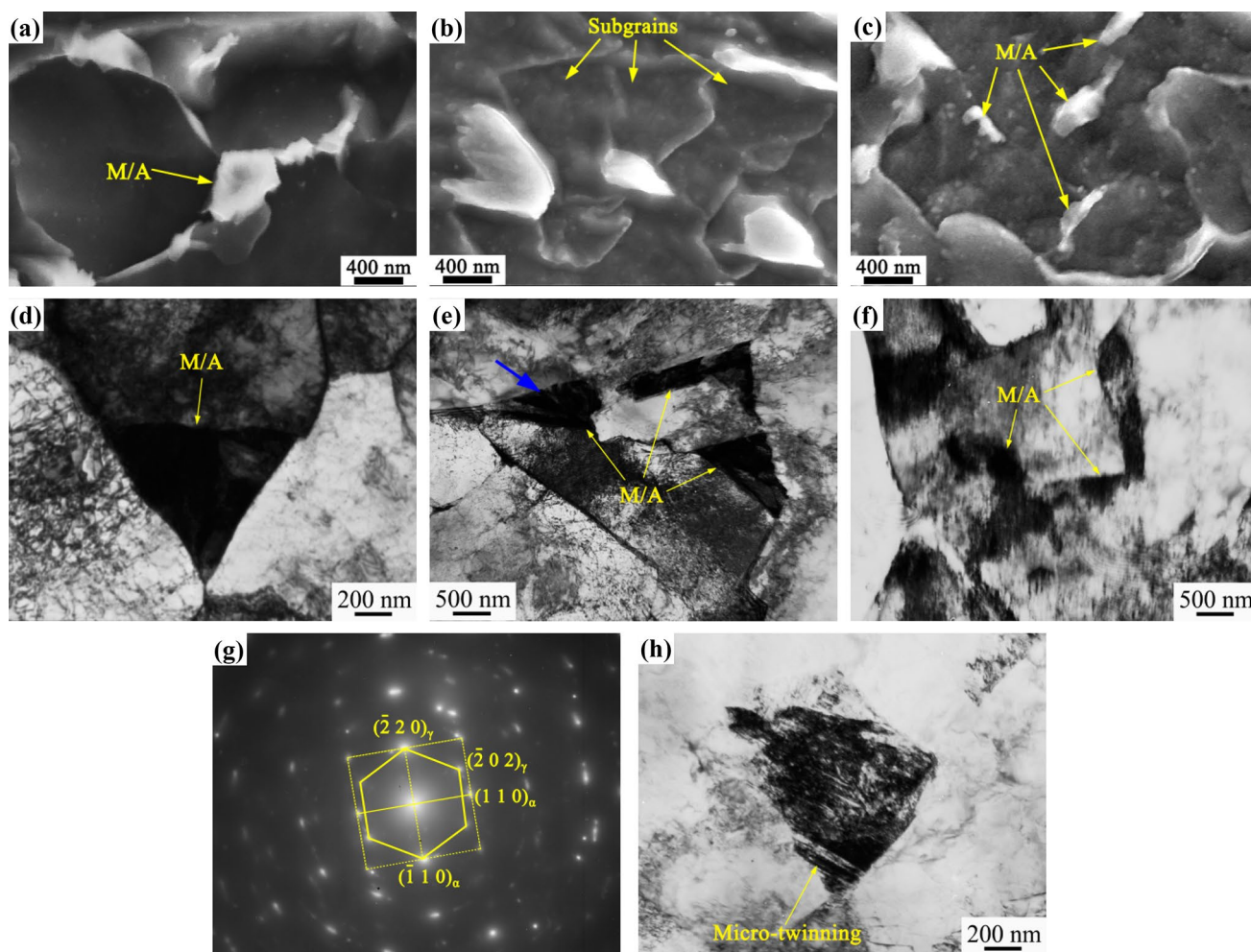
Fig. 7 Different morphologies of M/A constituent at medium cooling rate. **a–c** SEM morphology of M/A constituent formed on grain boundary nodes, subgrain boundaries and matrix interior, respectively; **d–f** TEM morphology of M/A constituent formed on grain boundaries, subgrain boundaries and matrix interior, respectively; **g** selected area diffraction patterns of M/A constituent in Fig. 7e marked by blue arrow; **h** M/A constituent with micro-twinning

as BF, AF and QF [33]. In the present work, for investigating the crystallography feature of M/A constituents alone, phase identification via the mean band contrast (MBC) function of EBSD was performed. The MBC function, derived from the BC distribution, is defined as the grain mean of a BC difference between adjoining pixels and can represent the local BC variations, which is easier to distinguish the critical values of different phases than BC [34]. The BC or MBC value is sensitive to the quality of the pattern. Commonly, the phase with high defect density (like the martensite) or internal stress (like the deformed microstructure) has a low pattern quality, which will have a small BC or MBC values.

The austenite was excluded from the calculation due to its negligible content. Thus, in the current situation, the phase identification of the M/A constituents could be simplified to the martensite identification. Then, the MBC curve was acquired and fitted by three Gaussian peaks, as displayed in

Fig. 8b. Grains with MBC value > 67, which is on the left of the first Gaussian peak with blue dash line, were treated as one of the threshold values for distinguishing the martensite phase. Meanwhile, the green dot line and yellow dash dot line could be treated as bainite and ferrite, respectively. However, when the martensite fraction is too small or the bainite exists, BC fraction alone may not be sufficient [34].

By measuring the size of the M/A constituent in Figs. 4, 7 and 8 through the Image J software, the M/A constituent size was approximately less than 1.5 μm, which was used for another criterion. Similarly, Caballero et al. [17] also reported that the grain size of M/A constituents in GB was about 1.5 μm.

Finally, setting the two criterions as the subsets in EBSD, the M/A constituents were identified by intersecting the two sunsets, as shown in Fig. 8c marked by the black areas. The black lines represent high-angle grain
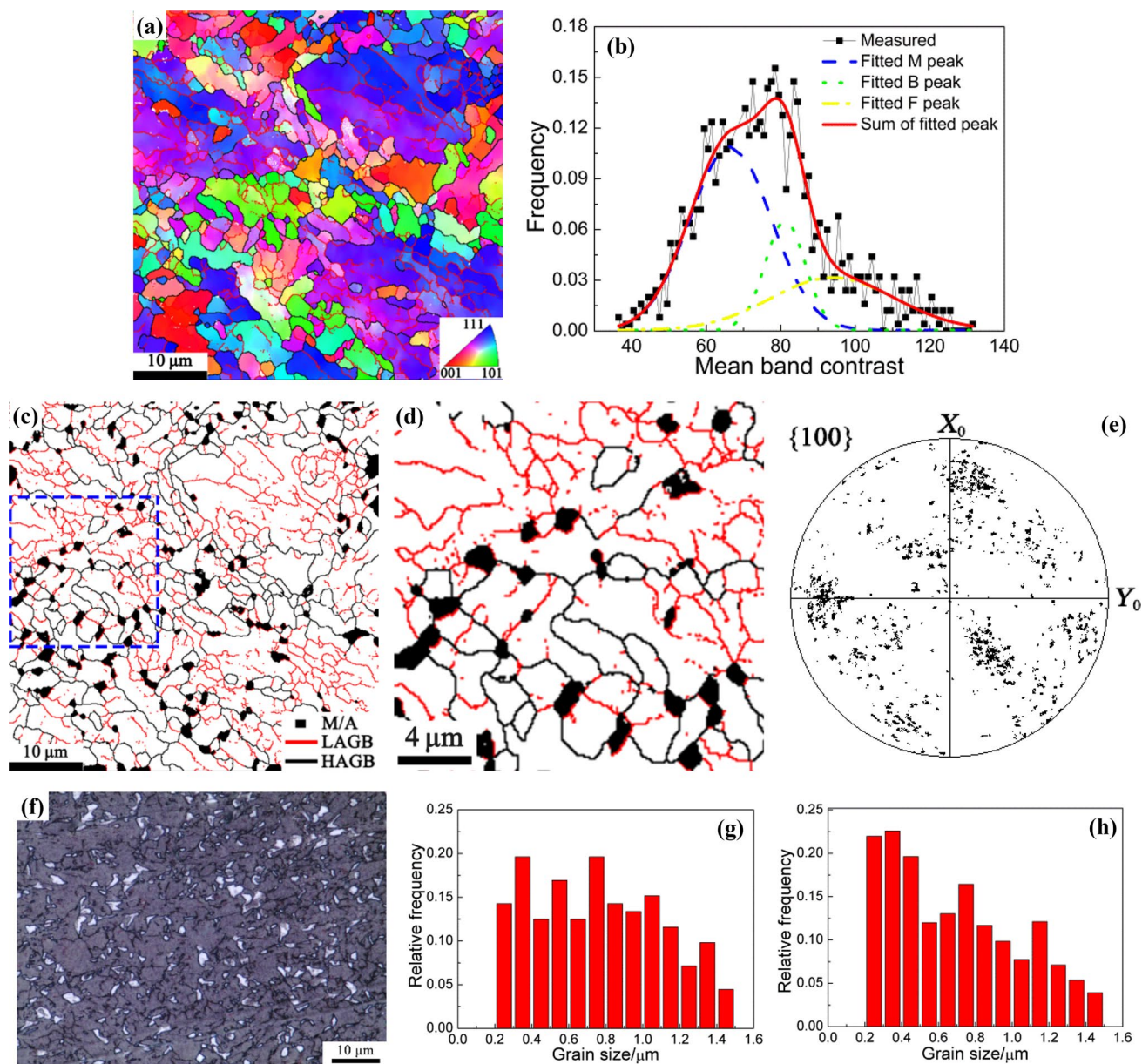
Fig. 8 EBSD results of sample at 40 °C/s. **a** Inverse pole figure; **b** mean band contrast distribution with Gaussian fit; **c** misorientation maps combined with M/A constituent; **d** enlarged part indicated by dashed box in **c**; **e** {100} pole figure of M/A constituent in **c**; **f** optical micrograph of M/A constituent etched by Lepera etchant; **g**, **h** distribution of M/A constituent in **c** and **f**, respectively

boundaries (HAGB) with a critical angle of > 15°, and the red lines represent low-angle grain boundaries (LAGB) with a critical angle between 2° and 15°. An enlarged part indicated by the box in Fig. 8c is shown in Fig. 8d. It is found that the M/A constituents were mainly formed on the boundary nodes in agreement with the results from SEM and TEM. Interestingly, some M/A constituents distributed along the grain boundaries enclosed partly by HAGBs and partly by LAGBs, which could be concluded that some martensite in M/A constituents misoriented from the adjacent ferrites with quite small misorientation angles. This is consistent with the results proposed by the

previous study that the GB generally contains the low-angle boundaries [32]. It is reported that the major alloying elements such as Mn, Ni and Cr could segregate at the interface between M/A constituents and QF surrounded by HAGBs, which deteriorated the critical crack tip opening displacement [32]. In contrast, the small orientation relationship between M/A constituents and GB matrix and the existence of abundant substructures make the distribution of elements more dispersive. In addition, the difference in microhardness between M/A constituents and soft ferrite matrix produces the M/A constituents with more voided or cracked in QF than that in GB [26]. This conclusion

also suggests that GB microstructure formed at medium cooling rate would have good toughness.

Furthermore, the {100} pole figure of the M/A constituents in Fig. 8c is solely displayed in Fig. 8e. A number of M/A grains had similar orientation, indicating that the martensite transformed from the carbon-enriched austenite in M/A constituents followed a certain orientation relationship.

For comparing with the EBSD characterization, the M/A constituents with bright white color were also revealed alone by the Lepera etchant in Fig. 8f. The M/A fraction in Fig. 8c, f was 4.0% and 5.9% (obtained by the EBSD and Image J software), respectively. Then, Fig. 8g, h shows the distribution of M/A constituents measured from Fig. 8c, f, respectively. The low M/A fraction measured by EBSD should be attributed to the process of eliminating noise. The high-carbon martensite consists of numerous micro-twinning or high dislocations resulting in indexing failures (no solution), and therefore, it is mistakenly deleted [26, 34]. In addition, there were also a few individual grains with the size over 1.5 µm and were not taken into account. However, despite certain errors existing, the MBC function could still be used to characterize the M/A constituents in GB qualitatively or semiquantitatively.

4 Conclusions

1. The ferrite matrix morphology of GB changes from the lath sheaf structures partly or completely surrounded by PAGB to the equiaxed-like large grains with the cooling rate decreasing from high (60 °C/s) to low (5–10 °C/s).

2. At the medium cooling rate (20–40 °C/s), GB shows the irregular refined ferrite matrix, the granular M/A constituents and abundant substructures inside. The formation of the irregular ferrite and substructures was attributed to the high-temperature recovery of the deformed austenite before phase transformation at the medium cooling rate. The granular morphology of M/A constituents was formed from the carbon-rich triple junctions that were produced by the multidirectional substructure interfaces converged with each other.

3. At the medium cooling rate, the M/A constituents in GB distributed on the boundary notes, subgrain boundaries and matrix interior can be found. Some martensite in M/A constituents misoriented from the adjacent ferrites by very small misorientation angles. The MBC function of EBSD could contribute to characterizing the M/A constituents qualitatively or semiquantitatively.

References

[1] Z.X. Qiao, Y.C. Liu, L.M. Yu, Z.M. Gao, J. Alloy. Compd. 475 (2009) 560–564.
[2] G. Krauss, S.W. Thompson, ISIJ Int. 35 (1995) 937–945.
[3] E.V. Morales, R.A. Silva, I.S. Bott, S. Paciornik, Mater. Sci. Eng. A 585 (2013) 253–260.
[4] Q.B. Yu, G.S. Duan, Y. Sun, X.P. Zhao, B. Wang, Iron and Steel 43 (2008) No. 7, 68–71.
[5] C.H. Lee, H.K.D.H. Bhadeshia, H.C. Lee, Mater. Sci. Eng. A 360 (2003) 249–257.
[6] R.Y. Zhang, J.D. Boyd, Metall. Mater. Trans. A 41 (2010) 1448–1459.
[7] C.J. Cheng, X.M. Wang, Z.J. Zhou, X. Liang, C.L. Miao, X.L. He, Acta Metall. Sin. 44 (2008) 287–291.
[8] Y.T. Zhao, C.J. Shang, S.W. Yang, X.M. Wang, X.L. He, Mater. Sci. Eng. A 433 (2006) 169–174.
[9] W. Wang, Y. Shan, K. Yang, Mater. Sci. Eng. A 502 (2009) 38–44.
[10] M.A. Smirnov, I.Y. Pyshmintsev, A.N. Boryakova, Metallurgist 54 (2010) 7–8.
[11] J.P. Wang, Z.G. Yang, B.Z. Bai, H.S. Fang, Mater. Sci. Eng. A 369 (2004) 112–118.
[12] W. Wang, W. Yan, L. Zhu, P. Hu, Y. Shan, K. Yang, Mater. Des. 30 (2009) 3436–3443.
[13] L. Fan, D.H. Zhou, T.L. Wang, S.R. Li, Q.F. Wang, Mater. Sci. Eng. A 590 (2014) 224–231.
[14] M.C. Zhao, K. Yang, F.R. Xiao, Y.Y. Shan, Mater. Sci. Eng. A 355 (2003) 126–136.
[15] H.J. Jun, J.S. Kang, D.H. Seo, K.B. Kang, C.G. Park, Mater. Sci. Eng. A 422 (2006) 157–162.
[16] S.W. Thompson, D.J. Colvin, G. Krauss, Metall. Mater. Trans. A 27 (1996) 1557–1571.
[17] F.G. Caballero, H. Roelofs, S. Hasler, C. Capdevila, J. Chao, J. Cornide, C. Garcia-Mateo, Mater. Sci. Technol. 28 (2012) 95–102.
[18] S. Zajac, V. Schwinn, K.H. Tacke, Mater. Sci. Forum 500–501 (2005) 387–394.
[19] Y.M. Kim, H. Lee, N.J. Kim, Mater. Sci. Eng. A 478 (2008) 361–370.
[20] J. Hu, L.X. Du, J.J. Wang, H. Xie, C.R. Gao, R.D.K. Misra, Mater. Sci. Eng. A 585 (2013) 197–204.
[21] F.R. Xiao, B. Liao, G.Y. Qiao, C.L. Zhang, Y.Y. Shan, Y. Zhong, K. Yang, Multidiscip. Model. Mater. Struct. 2 (2006) 389–410.
[22] Z.G. Yang, H.S. Fang, Curr. Opin. Solid State Mater. Sci. 9 (2005) 277–286.
[23] H.S. Fang, C. Feng, Y.K. Zhang, Z.G. Tang, B.Z. Bai, J. Iron Steel Res. Int. 15 (2008) No. 6, 1–9.
[24] P. Cizek, Acta Mater. 106 (2016) 129–143.
[25] D.P. Cheprasov, V.V. Svishchenko, E.V. Kozlov, A.A. Ivanaiskii, Met. Sci. Heat Treat. 5 (2006) 3–7.
[26] M. Mohammadijoo, J. Valloton, L. Collins, H. Henein, D.G. Ivey, Mater. Charact. 142 (2018) 321–331.
[27] N. Huda, A. R.H. Midawi, J Gianetto, R. Lazor, A.P. Gerlich, Mater. Sci. Eng. A 662 (2016) 481–491.
[28] C.M. Wang, X.F. Wu, J. Liu, N.A. Xu, Mater. Sci. Eng. A 438–440 (2006) 267–271.
[29] B.Z. Li, C.S. Li, X. Jin, J. Zhang, J. Iron Steel Res. Int. (2019-3-12). https://doi.org/10.1007/s42243-019-00244-8.
[30] B. Wang, J. Lian, Mater. Sci. Eng. A 592 (2014) 50–56.
[31] Y.W. Chen, Y.T. Tsai, P.Y. Tung, S.P. Tsai, C.Y. Chen, S.H. Wang, J.R. Yang, Mater. Charact. 139 (2018) 49–58.
[32] S.G. Lee, S.S. Sohn, B. Kim, W.G. Kim, K.K. Um, S. Lee, Mater. Sci. Eng. A 10 (2018) 1–21.
[33] H. Zhao, B.P. Wynne, E.J. Palmiere, Mater. Charact. 123 (2017) 339–348.
[34] J.Y. Kang, D.H. Kim, S. Baik, T.H. Ahn, Y.W. Kim, H.N. Han, K.H. Oh, H.C. Lee, S.H. Han, ISIJ Int. 51 (2011) 130–136.